PCCP

Site-Dependent Selectivity in Oxidation Reactions on Single Pt Nanoparticles

Journal:	*Physical Chemistry Chemical Physics*
Manuscript ID	CP-COM-02-2020-000642.R1
Article Type:	Communication
Date Submitted by the Author:	12-Mar-2020

Complete List of Authors:	Dery, Shahar; The Hebrew University of Jerusalem, Institute of Chemistry Kim, Suhong; UC Berkeley, Chemistry Mehlman, Hillel; The Hebrew University of Jerusalem, Institute of Chemistry Feferman, Daniel; The Hebrew University of Jerusalem, Institute of Chemistry Toste, F.; University of California, Chemistry Gross, Elad; The Hebrew University of Jerusalem, Institute of Chemistry

COMMUNICATION

Site-Dependent Selectivity in Oxidation Reactions on Single Pt Nanoparticles

Received 00th January 20xx,
Accepted 00th January 20xx

DOI: 10.1039/x0xx00000x

Shahar Dery[a], Suhong Kim[b], Daniel Feferman[a], Hillel Mehlman[a], F. Dean Toste[b] and Elad Gross*[a]

Site-dependent selectivity in oxidation reactions on Pt nanoparticles was identified by conducting IR nanospectroscopy measurements while using allyl-functionalized N-heterocyclic carbenes (allyl-NHCs) as probe molecules. Following exposure to oxidizing conditions the allyl groups in NHCs that were located on the center of Pt nanoparticles were oxidized to hydroxyl while those located on the nanoparticle's periphery were oxidized into carboxylic acid. The superior reactivity on the periphery of the nanoparticles was correlated to higher density of low coordinated atoms on these surface sites.

Heterogeneous catalysis is a surface-controlled phenomenon governed by low-coordinated sites such as steps and point defects.[1-7] Different surface sites often show variations in reactivity, leading to multiple reaction pathways and various products formation. This effect poses a major complication for the chemical industry owing to the high costs of products separation.[8-12] Therefore, gaining insights into the ways by which different surface sites direct the selectivity of catalytic nanoparticles is of fundamental importance.

The structural variation between catalytic nanoparticles along with the presence of dissimilar reactive sites on single nanoparticles makes it challenging to resolve their site dependent selectivity using ensemble-based spectroscopy measurements.[13-15] High spatial resolution techniques, such as super-resolution fluorescence microscopy[16-19] and tip-enhanced Raman spectroscopy (TERS)[20-26] were utilized for identifying catalytic reactions at the nanoscale.

Synchrotron-based IR nanospectroscopy (SINS) has been recently identified as a novel approach for high spatial resolution detection of chemical transformations on the surface of catalytic nansoparticles.[27-31] SINS is an Atomic-Force-Microscopy (AFM) based apertureless method which utilizes synchrotron-sourced IR light to overcome the diffraction limit of light and collect surface-scattered IR signal with a tip-limited spatial resolution of 20 nm.[32-35] As a result of its highly localized detection capabilities, SINS measurements were applied for identifying the local properties of polymers,[36] 2D materials,[37, 38] biomaterials[39] and catalysts.[28, 29]

It was previously demonstrated that catalytically-active sites can be mapped on single nanoparticles by conducting SINS measurements while using N-heterocyclic carbenes (NHCs) as probe molecules.[28, 29] The high chemical versatility of NHCs and their affinity to metal surfaces make them exceptional chemical indicators for surface-induced reactivity.[40, 41] By using addressable NHCs as markers and mapping their properties with localized SINS measurements it was revealed that the nanoparticle's periphery is more reactive than the flat regions located on the nanoparticle's center.[28] These site-dependent reactivity variations were correlated to higher density of low-coordinated surface atoms at the periphery of the nanoparticles.

SINS measurements provided so far direct information of site-specific *reactivity* on the surface of metallic nanoparticles.[28, 29] However, site-dependent *selectivity* was not detected yet by SINS measurements due to low concertation of intermediates on the metal surface, making their detection highly challenging. Herein, site dependent selectivity was identified in oxidation reaction on Pt nanoparticles by using allyl-functionalized NHCs (allyl-NHCs) as probe molecules (Scheme 1). The sequential transformation of the allyl groups to alcohol, a chemically-stable intermediate, and then to acid made it possible to locally monitor their site-dependent selectivity using IR nanospectroscopy.

[a] *Institute of Chemistry and The Centre for Nanoscience and Nanotechnology, The Hebrew University of Jerusalem, Jerusalem 91904, Israel*
[b] *Department of Chemistry, University of California, Berkeley, California 94720, United States*

† Footnotes relating to the title and/or authors should appear here.
Electronic Supplementary Information (ESI) available: [details of any supplementary information available should be included here]. See DOI: 10.1039/x0xx00000x

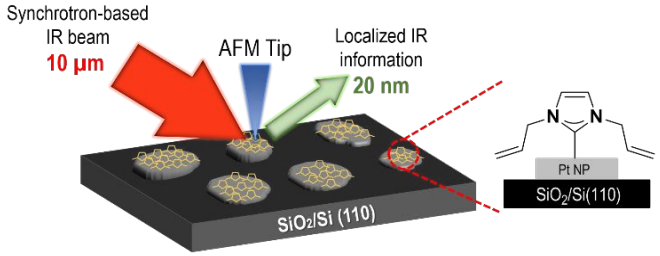

Scheme 1. Schematic illustration of the experimental approach. Allyl-functionalized NHCs (marked with orange pentagons) were anchored to the surfaces of Pt nanoparticles (grey circles), functioning as probe molecules for identifying site-dependent selectivity in oxidation reactions. High spatial resolution synchrotron infrared nanospectroscopy (SINS) measurements were performed to identify site-dependent selectivity on Pt particles.

Pt nanoparticles with an average size of 100 ± 30 nm were prepared by annealing (923 K, 5 h, 1 atm N_2) a 15 nm thick Pt film that was deposited on SiO_2/Si(110) wafer (Supp. Info. Fig. S1). Allyl-functionalized imidazolium salt was synthesized, deprotonated and anchored on the surface of Pt nanoparticles (additional experimental details can be found in the supporting information). The surface-anchoring of NHCs did not induce noticeable changes in the nanoparticles' morphology (Supp. Info. Fig. S1).

N1s XPS signal of the allyl-functionalized imidazolium salt, prior to its deprotonation and surface anchoring, revealed a sharp peak that was centered at 401.8 eV (Fig. 1, bottom spectrum).[42] N1s XPS signal of the surface-anchored allyl-NHC showed a broader peak that was centered at 399.1 eV.[43, 44] The shift in the peak position following deprotonation and surface-anchoring of the imidazolium salt was correlated to neutralization of the positive charge in the surface-anchored NHCs.[29, 40, 41]

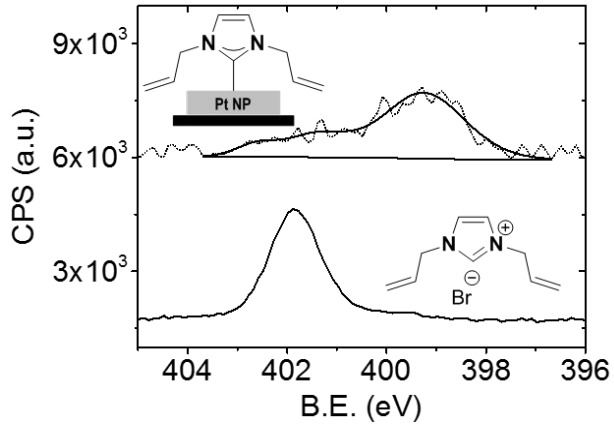

Figure 1. N1s XPS signals of allyl-functionalized imidazolium salt before (bottom spectrum) and after its activation and anchoring on Pt nanoparticles (top spectrum)

SINS measurements of Pt nanoparticles that were decorated with allyl-NHCs were conducted prior and following their exposure to oxidizing conditions. AFM topography measurement of NHCs-coated Pt nanoparticle was performed (Fig. 2i, AFM image). The topography measurement was followed by SINS measurements on different surface sites that probed the local vibrational signatures of surface-anchored allyl-NHCs. SINS measurement was performed at the center of Pt nanoparticle (measurement position was marked with a black circle in the AFM image in Fig. 2i). Vibrational peaks were detected at 1460 and 1550 cm^{-1} (Fig. 2i, black-colored spectrum) and attributed to C-H bending and C=C stretching, respectively. These two signals were probed as well in the IR spectrum of the allyl-functionalized imidazolium salt (Supp. Info. Fig. S2). The similarity in the IR signals of the imidazolium salt and the surface-anchored NHCs indicates that the allyl-NHCs were attached to Pt nanoparticles without major changes in the properties of their addressable allylic groups.

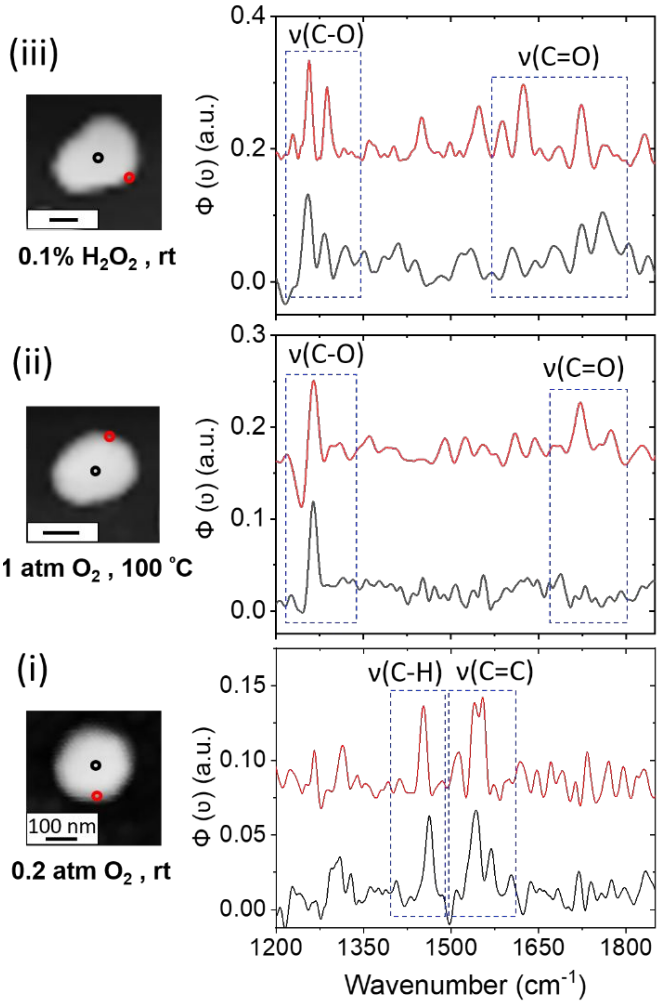

Figure 2. AFM topography images (left panels) and localized SINS spectra (right panels) of Si-supported Pt nanoparticles that were coated with allyl-NHCs. SINS measurements were performed following deposition of NHCs (i) and after exposure to gas phase (1 atm O_2, 100 °C, 10 h) (ii) and liquid phase (0.1 w/w% H_2O_2, rt, 10 h) oxidizing conditions (iii). SINS measurements were conducted at the center and side of Pt particles. Colored circles in the AFM topography image mark the SINS measurements position. The same color-coding is used for SINS spectra, correlating the SINS spectra with the specific measurement position. Scale bar is identical for the three AFM topography images.

SINS measurement was performed on the particle's perimeter (measurement position was marked with a red circle in the AFM image in Fig. 2i) and yielded an IR spectrum with two dominant peaks (red-colored spectrum in Fig. 2i). The SINS spectrum that was measured on the particle's periphery was similar to the one measured on the center of the nanoparticle. The resemblance of the two spectra implies that under ambient conditions the allyl-functionalized NHCs were stable and inert on both the center and edge of the nanoparticle.

The NHCs-coated Pt nanoparticles were exposed to gas-phase oxidizing conditions (1 atm O_2, 100 °C, 10 h) and their site-dependent reactivity was analyzed by SINS measurement. SINS spectrum was measured on the center of a single Pt nanoparticle (Fig. 2ii, black-colored spectrum, SINS measurement location was marked with a black circle in the AFM image) and showed a distinctive peak at 1265 cm^{-1}, which is corresponding to a C-OH stretch. The detection of this vibrational feature indicated that the allylic groups were oxidized to hydroxyls after exposure to oxidizing conditions.[45] The lack of C=C stretches in the SINS spectrum can be correlated to changes in the orientation of the NHC's imidazole ring that was shifted from standing into flat-lying position.[40, 41]

SINS spectrum was measured on the nanoparticle's periphery (marked with red circle in the AFM image in Fig. 2ii) and displayed two peaks that were located at 1265 and 1720 cm^{-1} (Fig. 2ii, red-colored spectrum), correlated to C-OH and C=O stretches, respectively. This result shows that the allyl groups in NHCs that were located at the edge of the nanoparticle were oxidized to carboxylic acid. Thus, partial oxidation of the allyl groups into alcohol was observed on the less-reactive flat regions of the nanoparticle while oxidation to acid was observed on the particle's edge. The enhanced reactivity on the periphery of the nanoparticles was correlated to higher density of low-coordinated atoms on these surface sites.[28, 30]

SINS measurements did not exclusively identify the presence of aldehyde on Pt nanoparticles as indicated by the coupled detection of vibrational features at the CO-H and C=O ranges (1200-1350 and 1600-1800 cm^{-1}, respectively). Aldehyde signal was not detected as well in NHCs that were functionalized with alcohol groups and exposed to oxidizing conditions.[29] The lack of aldehyde signal can be correlated to low surface concentration of this species due to its high reactivity on Pt under oxidizing conditions.

The NHC-coated Pt nanoparticles were exposed to harsher liquid-phase oxidizing conditions (0.1% w/w H_2O_2, rt, 10 h). SINS measurement was performed at the center of a single Pt particle (measurement location was marked with a black circle in the AFM image in Fig. 2iii) and yielded a spectrum with several peaks (black-colored spectrum, Fig. 2iii). The presence of several vibrational peaks demonstrates the less selective and more destructive nature of the harsher oxidizing conditions. The region between 1200 and 1300 cm^{-1} displayed one dominant peak at 1250 cm^{-1}, correlated to C-OH stretch. The region between 1550-1800 cm^{-1} exhibited several peaks with two dominant features at 1720 and 1760 cm^{-1}, which can be correlated to carboxylic acid and ester groups. These results indicate that exposure to harsher oxidizing conditions further facilitated the oxidation of the allyl groups in surface-anchored NHCs.

SINS measurement on the particle's edge, following exposure to liquid-phase oxidizing conditions, yielded an IR spectrum with several vibrational features (red circle in the AFM image in Fig. 2iii and the corresponding red-colored spectrum). Peaks at 1255 and 1725 cm^{-1} were assigned to C-OH and C=O vibrations of a carboxylic acid. Similar spectral features were obtained on these sites after exposure of the sample to gas-phase oxidizing conditions (Fig. 2ii). Spectral features were also detected at 1290 cm^{-1} and 1550-1620 cm^{-1}, attributed to partial decomposition of the NHCs that induced amide group formation. Partial decomposition and amide formation were previously identified in hydroxyl-functionalized NHCs that were anchored on Pt nanoparticles and exposed to harsh oxidizing conditions.[29] The localized SINS measurements therefore reveal that allyl groups of NHCs that were located on the edges of the particle show higher reactivity under both liquid and gas phase oxidizing conditions. Pt4f XPS measurements did not show variations in the oxidation state of the nanoparticles following their exposure to oxidizing conditions.

XPS measurements were conducted to complement the local near-field SINS data (Fig. 3). C1s XPS signal of the as-deposited allyl-NHCs (black-colored spectrum, Fig. 3) was fit by three Gaussians, centered at 284.8, 286.5 and 288.4 eV, and assigned to C-C, C-O and C=O species with a spectral weight of 85, 12 and 3%, respectively. The detection of C-O and C=O species indicated that some oxidation had already occurred following deposition of the allyl-NHCs on Pt nanoparticles, as was previously detected for OH-functionalized NHCs.[29] The low concertation of the oxidized species hindered their detection by the localized SINS measurements.

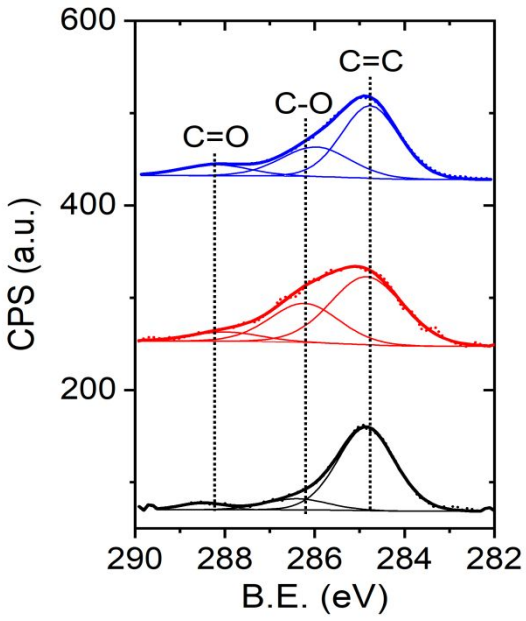

Figure 3. C1s XPS signals of allyl-functionalized NHCs that were anchored on Si-supported Pt nanoparticles. XPS measurements were conducted before (black colored spectrum) and after exposure of the sample to gas phase (1 atm O_2, 100 °C, 10 h, red colored spectrum)

and liquid phase (0.1% w/w H_2O_2, rt, 10 h, blue colored spectrum) oxidizing conditions. Gaussians were fit to each XPS signal.

The C1s XPS signal showed an increase in the C-O and C=O features, reaching a spectral weight of 40% after exposure of the sample to gas phase oxidizing conditions (red-colored spectrum, Fig. 3). This change in the XPS pattern was correlated with variations in the SINS data (Fig. 2) that identified the oxidation of the allylic groups into hydroxyl and carboxylic acid. C1s XP spectrum ensuing liquid phase oxidizing conditions (blue-colored spectrum, Fig. 3) showed a spectral weight of 63%, 27%, 10% for the C-C, C-O and C=O species, respectively. The increased weight of the C=O species corroborates the SINS data which indicated an amide formation in addition to allyl oxidation to carboxylic acid following exposure to harsher liquid phase oxidizing conditions.

To conclude, site-dependent selectivity in oxidation reactions was identified by using allyl-functionalized NHCs as molecular markers and mapping their reactivity on Pt nanoparticles with high spatial resolution IR nanospectroscopy measurements. Under gas phase oxidizing conditions the allyl groups of NHCs that were located at the periphery of Pt nanoparticles were fully oxidized to carboxylic acid, whereas the allyl groups of NHCs that were located at the center of the nanoparticle were oxidized into hydroxyl. Following exposure to harsher liquid-phase oxidizing conditions the allylic groups throughout the nanoparticle were oxidized to carboxylic acid and partial decomposition of NHCs was detected at the particle's edge. The enhanced reactivity that was probed at the particle's periphery suggests that higher density of surface defects facilitated the dissociative chemisorption of O_2 on these surface sites.[46] The site-dependent selectivity of surface-anchored NHCs, which was demonstrated in this work, can be further utilized for identifying the influence of surface composition on the reactivity[47] and for tuning the local molecular environment of catalytic nanoparticles.[48]

Conflicts of interest

There are no conflicts to declare.

Acknowledgments

This research was partially supported by the European Research Council (ERC) under the European Union's Horizon 2020 research and innovation program (Grant Agreement No. 802769, ERC Starting Grant "MapCat"). S.D. acknowledges the Israeli Ministry of Energy and the Azrieli foundation for financial support. F.D.T. thanks the Director, Office of Science, Office of Basic Energy Sciences and the Division of Chemical Sciences, Geosciences, and Biosciences of the US Department of Energy at LBNL (DE-AC02-05CH11231) for partial support of this work. The Advanced Light Source is supported by the Director, Office of Science, Office of Basic Energy Sciences, of the US Department of Energy under contract number DE-AC02-05CH11231. We acknowledge the assistance of Dr. Hans Bechtel (Advanced Light Source, Lawrence Berkeley National Lab) in conducting the SINS experiments.

References

1. G. Ertl and H.-J. Freund, *Physics Today*, 1999, **52**, 32-38.
2. G. Somorjai, in *Advances in catalysis*, Elsevier, 1977, vol. 26, pp. 1-68.
3. G. Somorjai and D. Blakely, *Nature*, 1975, **258**, 580.
4. J. r. m. D. Pelletier and J.-M. Basset, *Accounts of chemical research*, 2016, **49**, 664-677.
5. A. Vojvodic and J. K. Nørskov, *National Science Review*, 2015, **2**, 140-143.
6. E.-J. Ras and G. Rothenberg, *RSC Advances*, 2014, **4**, 5963-5974.
7. B. Roldan Cuenya and F. Behafarid, *Surface Science Reports*, 2015, **70**, 135-187.
8. A. Corma, *Angewandte Chemie International Edition*, 2016, **55**, 6112-6113.
9. A. T. Bell, *Science*, 2003, **299**, 1688-1691.
10. J. K. Nørskov, T. Bligaard, B. Hvolbæk, F. Abild-Pedersen, I. Chorkendorff and C. H. Christensen, *Chemical Society Reviews*, 2008, **37**, 2163-2171.
11. I. Atadashi, M. Aroua and A. A. Aziz, *Renewable Energy*, 2011, **36**, 437-443.
12. F. Cavani and J. H. Teles, *ChemSusChem: Chemistry & Sustainability Energy & Materials*, 2009, **2**, 508-534.
13. F. Zaera, *Progress in Surface Science*, 2001, **69**, 1-98.
14. B. M. Weckhuysen, *Physical Chemistry Chemical Physics*, 2003, **5**, 4351-4360.
15. H. Topsøe, *Journal of Catalysis*, 2003, **216**, 155-164.
16. P. Chen, X. Zhou, H. Shen, N. M. Andoy, E. Choudhary, K.-S. Han, G. Liu and W. Meng, *Chemical Society Reviews*, 2010, **39**, 4560-4570.
17. N. Zou, X. Zhou, G. Chen, N. M. Andoy, W. Jung, G. Liu and P. Chen, *Nature chemistry*, 2018, **10**, 607.
18. M. B. Roeffaers, G. De Cremer, H. Uji-i, B. Muls, B. F. Sels, P. A. Jacobs, F. C. De Schryver, D. E. De Vos and J. Hofkens, *Proceedings of the National Academy of Sciences*, 2007, **104**, 12603-12609.
19. M. B. J. Roeffaers, G. De Cremer, J. Libeert, R. Ameloot, P. Dedecker, A.-J. Bons, M. Bückins, J. A. Martens, B. F. Sels, D. E. De Vos and J. Hofkens, *Angewandte Chemie International Edition*, 2009, **48**, 9285-9289.
20. E. M. van Schrojenstein Lantman, T. Deckert-Gaudig, A. J. Mank, V. Deckert and B. M. Weckhuysen, *Nature nanotechnology*, 2012, **7**, 583.
21. J.-H. Zhong, X. Jin, L. Meng, X. Wang, H.-S. Su, Z.-L. Yang, C. T. Williams and B. Ren, *Nature nanotechnology*, 2017, **12**, 132.
22. C. E. Harvey and B. M. Weckhuysen, *Catalysis letters*, 2015, **145**, 40-57.
23. N. Kumar, B. Stephanidis, R. Zenobi, A. J. Wain and D. Roy, *Nanoscale*, 2015, **7**, 7133-7137.
24. H. Kim, K. M. Kosuda, R. P. Van Duyne and P. C. Stair, *Chemical Society Reviews*, 2010, **39**, 4820-4844.
25. L. Q. Zheng, X. Wang, F. Shao, M. Hegner and R. Zenobi, *Angew Chem Int Edit*, 2018, **57**, 1025-1029.
26. N. Kumar, C. S. Wondergem, A. J. Wain and B. M. Weckhuysen, *J Phys Chem Lett*, 2019, **10**, 1669-1675.

27. Y. Levratovsky and E. Gross, *Faraday discussions*, 2016, **188**, 345-353.
28. C. Y. Wu, W. J. Wolf, Y. Levartovsky, H. A. Bechtel, M. C. Martin, F. D. Toste and E. Gross, *Nature*, 2017, **541**, 511-515.
29. S. Dery, S. Kim, D. Haddad, A. Cossaro, A. Verdini, L. Floreano, F. D. Toste and E. Gross, *Chem Sci*, 2018, **9**, 6523-6531.
30. S. Dery, E. Amit and E. Gross, *Top Catal*, 2018, **61**, 923-939.
31. E. Gross, *Nano Res*, 2019, **12**, 2200-2210.
32. H. A. Bechtel, E. A. Muller, R. L. Olmon, M. C. Martin and M. B. Raschke, *Proceedings of the National Academy of Sciences*, 2014, **111**, 7191-7196.
33. O. Khatib, H. A. Bechtel, M. C. Martin, M. B. Raschke and G. L. Carr, *ACS Photonics*, 2018, **5**, 2773-2779.
34. I. D. Barcelos, A. R. Cadore, L. C. Campos, A. Malachias, K. Watanabe, T. Taniguchi, F. C. Maia, R. Freitas and C. Deneke, *Nanoscale*, 2015, **7**, 11620-11625.
35. G. J. Ellis and M. C. Martin, *European Polymer Journal*, 2016, **81**, 505-531.
36. F. Huth, A. Govyadinov, S. Amarie, W. Nuansing, F. Keilmann and R. Hillenbrand, *Nano letters*, 2012, **12**, 3973-3978.
37. P. Li, T. Wang, H. Böckmann and T. Taubner, *Nano letters*, 2014, **14**, 4400-4405.
38. Z. Fei, A. Rodin, G. O. Andreev, W. Bao, A. McLeod, M. Wagner, L. Zhang, Z. Zhao, M. Thiemens and G. Dominguez, *Nature*, 2012, **487**, 82.
39. B. T. O'Callahan, K. T. Crampton, I. V. Novikova, T. Jian, C.-L. Chen, J. E. Evans, M. B. Raschke, P. Z. El-Khoury and A. S. Lea, *The Journal of Physical Chemistry C*, 2018, **122**, 24891-24895.
40. S. Dery, S. Kim, G. Tomaschun, I. Berg, D. Feferman, A. Cossaro, A. Verdini, L. Floreano, T. Kluner, F. D. Toste and E. Gross, *J Phys Chem Lett*, 2019, **10**, 5099-5104.
41. S. Dery, S. Kim, G. Tomaschun, D. Haddad, A. Cossaro, A. Verdini, L. Floreano, T. Kluner, F. D. Toste and E. Gross, *Chem-Eur J*, 2019, **25**, 15067-15072.
42. A. Rühling, K. Schaepe, L. Rakers, B. Vonhören, P. Tegeder, B. J. Ravoo and F. Glorius, *Angewandte Chemie International Edition*, 2016, **55**, 5856-5860.
43. C. M. Crudden, J. H. Horton, I. I. Ebralidze, O. V. Zenkina, A. B. McLean, B. Drevniok, Z. She, H.-B. Kraatz, N. J. Mosey and T. Seki, *Nature chemistry*, 2014, **6**, 409.
44. A. V. Zhukhovitskiy, M. G. Mavros, T. Van Voorhis and J. A. Johnson, *Journal of the American Chemical Society*, 2013, **135**, 7418-7421.
45. J. D. Burrington, C. T. Kartisek and R. K. Grasselli, *J Catal*, 1984, **87**, 363-380.
46. T. K. Slot, D. Eisenberg, D. van Noordenne, P. Jungbacker and G. Rothenberg, *Chemistry – A European Journal*, 2016, **22**, 12307-12311.
47. E. Gross and M. Asscher, *Langmuir*, 2010, **26**, 16226-16231.
48. E. Gross and G. A. Somorjai, *Top Catal*, 2014, **57**, 812-821.